Prediction and Observation of Electron Instabilities and Phase Space Holes Concentrated in the Lunar Plasma Wake

AGU100 ADVANCING EARTH AND SPACE SCIENCE

Geophysical Research Letters

RESEARCH LETTER
10.1029/2017GL076880

Key Points:
- The solar wind wake of the Moon is predicted to be unstable, leading to electron holes; satellite observations now confirm this prediction
- ARTEMIS observations of electrostatic fluctuations within 10 Moon radii show that electron holes are strongly concentrated in the Moon's wake
- The hole flux is observed to have a hollow profile in the wake, in qualitative agreement with the theoretical model

Supporting Information:
- Supporting Information S1
- Data Set S1
- Data Set S2

Correspondence to:
I. H. Hutchinson,
ihutch@mit.edu

Citation:
Hutchinson, I. H., & Malaspina, D. M. (2018). Prediction and observation of electron instabilities and phase space holes concentrated in the lunar plasma wake. *Geophysical Research Letters*, *45*, 3838–3845. https://doi.org/10.1029/2017GL076880

Received 19 DEC 2017
Accepted 7 APR 2018
Accepted article online 19 APR 2018
Published online 11 MAY 2018

Prediction and Observation of Electron Instabilities and Phase Space Holes Concentrated in the Lunar Plasma Wake

Ian H. Hutchinson[1] **and David M. Malaspina**[2]

[1]Plasma Science and Fusion Center, Massachusetts Institute of Technology, Cambridge, MA, USA, [2]Laboratory for Atmospheric and Space Physics, University of Colorado Boulder, Boulder, CO, USA

Abstract Recent theory and numerical simulation predicts that the wake of the solar wind flow past the Moon should be the site of electrostatic instabilities that give rise to electron holes. These play an important role in the eventual merging of the wake with the background solar wind. Analysis of measurements from the ARTEMIS satellites, orbiting the Moon at distances from 1.2 to 11 R_M, detects holes highly concentrated in the wake, in agreement with prediction. The theory also predicts that the hole flux density observed should be hollow, peaking away from the wake axis. Observation statistics qualitatively confirm this hollowness, lending extra supporting evidence for the identification of their generation mechanism.

Plain Language Summary Analysis of measurements by the ARTEMIS satellites orbiting the Moon shows that, in the lunar plasma wake, isolated electric structures called electron holes are being continuously formed. These holes are regions of depleted electron density that are maintained by their own positive charge. As the solar wind flows supersonically past the Moon, a density-depleted wake of approximate length 20,000 km (10 lunar radii) forms behind it. Plasma streams along the magnetic field fill in the wake, and theory predicts that instabilities should occur giving rise to these holes. They are solitary waves (solitons) consisting of short electric potential humps of width approximately 100 m. Motivated by this theory, ARTEMIS measurements of rapid variations of the electric field around the satellite have been searched for the characteristic signatures of holes. It is found that holes occur extremely frequently when the satellites are in the wake, but only very rarely outside the wake, and that in accordance with theory, the holes occur less frequently at the wake center than part-way out.

1. Introduction

The wake of supersonic plasma flow past a nonmagnetic body much larger than the Debye length, such as the solar wind past the Moon (and many other solar system bodies), has been predicted to be a source of instability and resulting electron holes (EHs)—that is, electrostatic solitary structures of the BGK type (Bernstein et al., 1957) sustained by an electron phase space deficit on trapped orbits (Hutchinson, 2017). Therefore, we have undertaken a systematic search for EHs in the abundant data from the ARTEMIS satellites (Angelopoulos, 2011), which frequently cross the Moon's wake, in order to test the predictions of the theory. The first results and comparisons are presented here.

The wake consists of a region of strongly depleted density immediately downstream of the body and an associated region of negative electric potential, which repels electrons and attracts ions, so as to maintain quasineutrality.

The density and potential well of the wake gradually fills over a characteristic distance downwake of approximately MR_M where $M = v_{\mathrm{wind}}/c_s$ is the Mach number of the external plasma flow and R_M is the body's transverse size (Moon radius). This process is governed predominantly by the ion dynamics. ARTEMIS observations confirm this general picture (Zhang et al., 2014) and also show broadband electrostatic noise in the lunar wake (Rubia et al., 2017).

The electron density remains close to Boltzmann, $n_e \simeq n_{e\infty} \exp(e[\phi - \phi_\infty])$, relative to its value in the external plasma (subscript ∞), because the electron cross-wake parallel transport, along the ambient magnetic field, is so fast compared with the ions. However, if instabilities do not intervene, the collisionless electron

velocity distribution does *not* remain Maxwellian. It develops a deep, but relatively narrow, "dimple" at a velocity corresponding to electrons whose parallel energy makes them approximately stationary at the (parallel) peak of the wake potential (Hutchinson, 2012). The dimple arises because of the approximate stagnation of these marginal electron orbits at the peak. The cross-field (downwake) drift of the plasma at the solar wind speed convects the electrons from the low-density (depleted) region to the higher (filled in) region. Nonstagnant electrons, which have much faster parallel velocities, are exchanged quickly with the surrounding rising density, and as a result, their distribution function is greater than it is for the stagnant orbits that started in a lower-density region. This creates the dimple—which causes electrostatic instability (Hutchinson et al., 2015) and is observed in simulations (Haakonsen et al., 2015) to lead to EHs.

2. Theoretical Predictions

A simple approximate model is to take the potential form along the parallel (to B) spatial coordinate x, to be invariant but the density in the well to be rising with a characteristic time-constant τ_r, as the orbit is convected downstream. (In this theoretical section, x is the coordinate determining cross-wake position, and position downwake is determined essentially by time t because the wake is taken to move downwake at the constant speed of the external solar wind.) External electrons are injected along the field from a growing parallel-velocity-distribution, $f(v_s) \propto \exp(t/\tau_r) f_M(x_s, v_s)$, where f_M is approximately Maxwellian in velocity shape, as representative of a broad electron distribution, and independent of time. This model yields an analytic solution for the distribution as follows. Express dimensionless electron velocities in units of $\sqrt{T_e/m_e}$, potential in units of T_e/e, where T_e is the external electron temperature, and time in units of inverse plasma frequency ω_{pe}^{-1}. Approximate the wake near its center as having parabolic potential $\phi = x^2/2x_c^2$, where x is the cross-wake distance parallel to the magnetic field from the wake center. An orbit's total energy (kinetic plus potential, accounting only for parallel velocity v), $\mathcal{E} = v^2/2 - \phi = (v^2 - x^2/x_c^2)/2 = v_0^2/2$ is then constant; and v_0 can be considered the orbit's velocity at $x = 0$ (where $\phi = 0$) and so v_0^2 is twice the total energy of the orbit, which is negative for reflected orbits and positive for passing orbits. Consequently, the relationship between time and parallel position x on an orbit is

$$t_x = \int^x \frac{\mathrm{d}x'}{v(x')} = \int^x \frac{\alpha \mathrm{d}x'}{\sqrt{(x'/x_c)^2 + v_0^2}} = \alpha x_c \ln\left[\sqrt{(x/x_c)^2 + v_0^2} + x/x_c\right], \tag{1}$$

where α is the sign of the velocity.

An orbit is considered to start at a position $x_s = \pm L$ (L being a constant of order the wake width) at time t_s and arrive at position x at time t_x. Then, the time delay is given by

$$\Delta t = t_x - t_s = \alpha_x x_c \left\{ \ln\left|\sqrt{(x/x_c)^2 + v_0^2} + x/x_c\right| + \alpha_R \ln\left|\sqrt{(x_s/x_c)^2 + v_0^2} + x_s/x_c\right| - (\alpha_R + 1)\ln|v_0| \right\}, \tag{2}$$

where $\alpha_R = 1$ for reflected, and -1 for (as yet) unreflected particles, and α_x is the velocity sign at x. Then, the distribution function can be written

$$\exp(\phi_s - \phi_x) f(v_x, x, t_x) = f_M(x_s, v_x) \exp(\Delta t/\tau_r), \tag{3}$$

where a constant of normalization has been omitted. This distribution is illustrated by the curves of Figure 1. It represents the actual distribution distortion—that is, the solution of Vlasov's equation—of the counterstreaming electrons entering the wake from a broad, single-humped, external velocity distribution.

The dimple distributions are unstable. In 1-D particle-in-cell simulations, the instabilities produce nonlinear vortices of trapped electrons in phase space that merge to form isolated EHs. Regions away from the holes then have dimples that are flattened so as to be linearly stable. Figure 2 illustrates an appropriate case. Applying the Penrose criterion (Penrose, 1960; determined by numerical integration) to distributions with

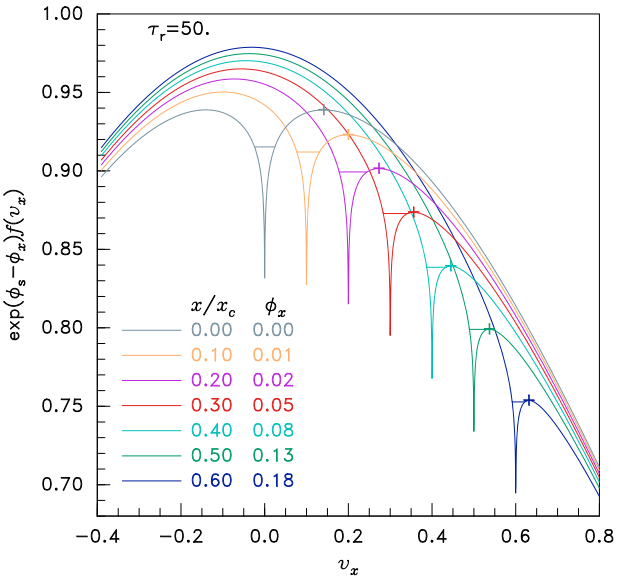

Figure 1. Dimple parallel-velocity distributions at various spatial positions x and hence potentials ϕ_x (when $\tau_r = 50x_c$, in normalized units, and $L = x_c$). Horizontal lines in the dimple indicate marginal stability levels.

the dimple partially filled in, the maximum level of the filling plateau that gives linear instability is found and drawn also in Figure 1. This shows how much of the dimple must be incorporated into EHs to maintain marginal stability. We find that for positions $x \gtrsim 0.25x_c$ ($\phi \lesssim -0.03T_e/e$), stabilization requires the dimple be filled out to the local maximum in the distribution (indicated by +), which is estimated analytically to be at energy $v_0^2/2 \simeq x_c/\tau_r$. The dimple minimum is at $v_0 = 0$, and because of the dimple asymmetry it is a reasonable approximation to ignore the smaller flattened region of reflected orbits. One then immediately obtains the phase space flux of holes as $\Gamma \simeq v_0^2/2 \simeq x_c/\tau_r$.

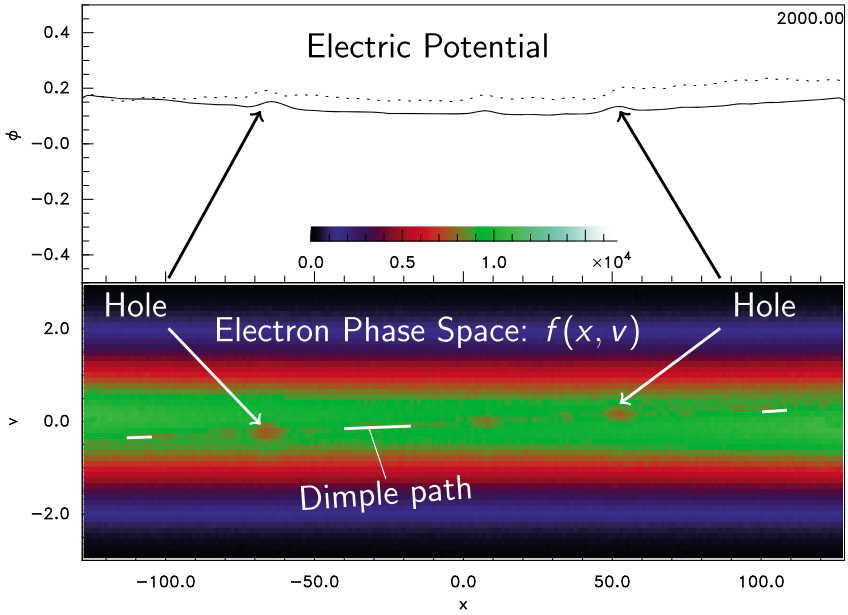

Figure 2. Example frame of hole formation in a rising density, parabolic potential, 1-D particle-in-cell simulation of a wake. Holes move outward from the center, along the "dimple path" in phase space. $t = 2,000/\omega_p$, $\tau_r = 10,000/\omega_p$, $x_c = 316\lambda_D$ ($\lambda_D = 1$).

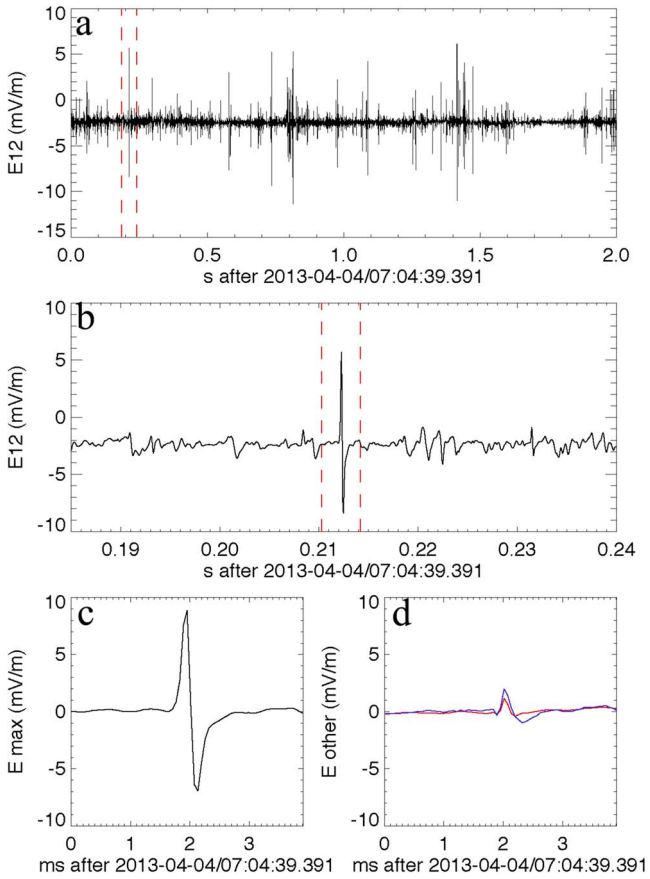

Figure 3. Example electron hole waveforms and algorithm detections. (a) Electric field measured by ARTEMIS P1 E_{12} during an EFI burst on 4 April 2013, in the lunar wake. (b) Portion of (a) indicated by vertical dashed lines in (a). (c) Maximum variance electric field over time indicated by vertical lines in (b). (d) Minimum variance (red) and mutually orthogonal electric fields (blue).

For $x \lesssim 0.25x_c$ the flattening required for nonlinear stabilization is incomplete and has a much smaller extent in v_0^2, which determines Γ. Therefore, the hole phase space flux is lower (typically $\sim 0.1x_c/\tau_r$ at $x = 0$), giving a Γ profile that is hollow.

Taking $x_c \sim L \sim R_M$ and using the previously mentioned characteristic wake length MR_M to determine $\tau_r \sim MR_M/Mc_s = R_M/c_s = \sqrt{m_i/m_e}R_M/v_{te}$, we find $\tau_r/x_c \sim \sqrt{m_i/m_e} \sim 50$ for hydrogen ions (in dimensionless units). These are the values used for Figure 1.

In broad terms, then, the theory of the dimple mechanism predicts that the lunar wake is a region of concentrated electrostatic electron instability, giving rise to EHs, whose motion is predominantly outward across the wake along the magnetic field. The flux of trapped electron phase space passing any point should be hollow, rising from a relatively small value at the wake axis to a saturated level at a distance (parallel to B) of about $\frac{1}{4}$ of the wake width.

3. Instrumentation and Data Analysis

ARTEMIS satellites P1 and P2 have, respectively, retrograde and prograde orbits about the Moon, with periapses of $\sim$ 1.2 lunar radii (R_M) and apoapses of $\sim 11R_M$ (from lunar center), and so cover one characteristic wake length for a wind Mach number of 10. Their orbital periods are $\sim$ 25 hr. We analyze data between 29 October 2011 and 13 September 2017, giving $\sim$ 4,000 (P1 + P2) wake crossings. These are spin-stabilized spacecraft with ~3-s spin period and spin planes roughly aligned with the ecliptic plane.

Two ARTEMIS instruments are used in this analysis. The Electric Field Instrument (EFI; Bonnell et al., 2008; Cully et al., 2008) and the ElectroStatic Analyzers (ESAs; McFadden et al., 2008). EFI measures electric fields using six probes at the ends of six booms. Spherical probes are used in the spin plane, separated by $\sim$ 50 and 40 m.

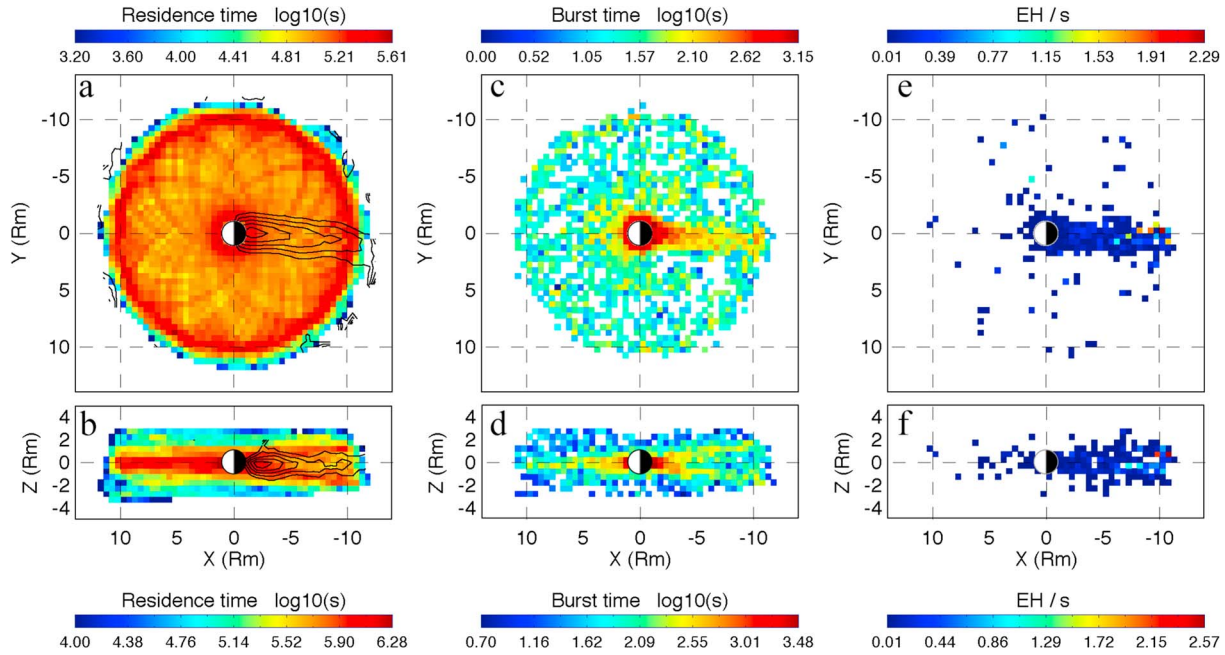

Figure 4. Spatial distribution of EH (29 October 2011 to 13 September 2017) relative to the Moon. (a) ARTEMIS P1 and P2 residence time for each *XY* grid square (integrated along *Z*). Proton density contours are overlaid. (c) Seconds of available burst data for *XY* grid square. (e) EH observed per second of burst data in each *XY* grid square. (b,d,f) Same as (a), (c), and (e) but for *XZ* grid squares (integrated along *Y*). EH = electron hole.

Cylindrical whips are used in the axial direction, ~7 m tip to tip. Only "dipole" data, consisting of the voltage difference between opposite probes, is analyzed here.

The ion ESA is used here only to determine the background density. The temporal resolution of the ESAs is much too slow to resolve hole fluctuations.

Our analysis makes use of the EFI high-resolution time series data, which consist of ~5- or ~ 10-s bursts of 16,384 samples per second of AC-coupled (>10 Hz), three-axis, electric field data E_{12}, E_{34}, and E_{56}. EFI burst data collection is triggered onboard based on the highest-amplitude signals in a specific frequency passband (Bonnell et al., 2008; Cully et al., 2008). A limited amount of automatically selected data is retained in onboard memory for transmission to Earth. The number of bursts returned per day is low (~3 per day is typical).

We must ensure that the solar wind lunar wake we sample is well outside the Earth's magnetosphere, whose tail and flanks are heavily populated with EHs generated by other mechanisms (e.g., double layers and magnetic reconnection; Andersson et al., 2009; Ergun et al., 2016). To accomplish this, ARTEMIS EFI burst data are considered only when the Moon is >20 Earth radii (R_E), in the geocentric solar equatorial (GSE) *Y* direction, away from a "typical" bow shock surface. This surface is defined using the Fairfield (1971) model with 4-nPa dynamic pressure and $|B| = 8$ nT oriented along the Parker spiral. The reduced data set contains 2,832 wake crossings.

The retained EFI burst data are broken into 1-s intervals and an automated algorithm (derived from Ergun et al., 2016) is applied for EH identification to each interval. "Peaks" are identified as times when electric field magnitude ($|E|$) derivative changes sign. Each peak is assigned a width defined by 4 times the number of waveform samples between the peak and the nearest adjacent peak. A peak is then considered isolated (representing a possible hole) if at ± 4.5 widths from the peak $|E|$ is ≤ 4 times its peak value. If so, it is retained and the vector electric field within the 9-width period about the peak is rotated into a maximum variance coordinate system. Since bipolar electric field pulses are the signature of an EH, we also require that the maximum-variance *E* component has a maximum and a minimum of opposite sign within 1 width, and these two stationary field absolute values can differ by no more than a factor of 2. The bipolar pulses identified by the algorithm are then examined by eye, and any remaining wave packets are removed. In our data selected to avoid the magnetosphere, the identification algorithm found 3,959 isolated bipolar EHs, in 68,686 s of high-cadence EFI burst data. Our algorithm discards many additional hole candidates in the data set, with strongly asymmetric electric field signatures or too closely spaced to readily distinguish from wave packets.

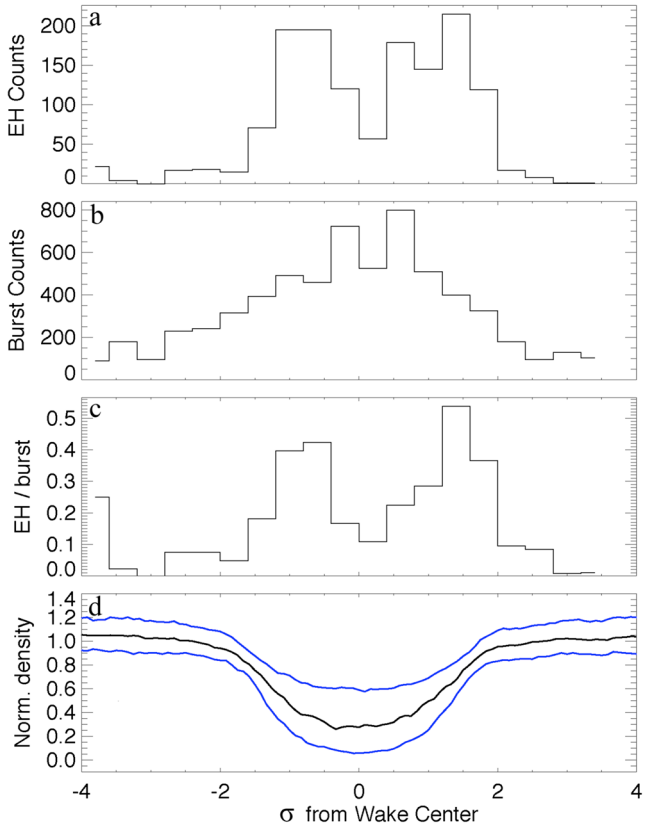

Figure 5. Occurrence of electron holes (EHs) and wake density as a function of normalized wake width (σ). (a) Histogram of EH events. See text for details. (b) Histogram of 1-s burst intervals. (c) Histogram of EH events observed per second of available burst data. (d) Normalized wake density, median (black) and quartiles (blue) for the 385 wake crossings included here.

4. Observations

Figure 3 illustrates an EH identified by the algorithm. Figure 3a shows the E_{12} electric field. Its region between vertical dashed lines is expanded in Figure 3b. Figure 3c shows the maximum variance electric field for 9 peak widths about the EH (indicated by vertical dashed lines in Figure 3b). Figure 3d shows the minimum variance (red) and mutually orthogonal (blue) electric fields. The EH waveform is consistent with prior EH observations (Andersson et al., 2009; Ergun et al., 1998; Malaspina et al., 2013; Matsumoto et al., 1994, 2003).

Figure 4 shows the spatial distribution of identified EHs near the Moon. Figure 4a shows seconds of ARTEMIS residence time in each 0.25 R_M by 0.25 XY grid square (integrated along Z). Positions are denoted by distances from the Moon in the GSE coordinate directions. X: toward the sun, Y: normal to X in the ecliptic plane, and Z: normal to the ecliptic. These coordinates (different from the x of our theory treatment) are conventionally used in lunar wake observations, for example (Zhang et al., 2014), and simulations, for example, (Birch & Chapman, 2001). Contours of normalized proton density (defined as the density time series data of each orbit divided by its median over the orbit) are overplotted. They show the wake extending in the direction of the solar wind ($-X$) but aberrated a few degrees from the optical wake by the 30 km/s orbital motion (in the Y direction) of the Earth and the Moon about the Sun. Figure 4b is similar to Figure 4a but for the XZ grid (integrated along Y).

Figures 4c and 4d show seconds of available EFI high cadence burst data per XY, XZ grid square. Burst data are densest within 1 R_M of the lunar surface, in a half-disk upstream of the Moon ($\lesssim 3\ R_M$ in radius), and throughout the plasma wake. This indicates that electrostatic plasma instabilities are concentrated there, because the EFI burst data system is triggered by high amplitude electric fields.

Figures 4e and 4f show the number of identified EHs, normalized by seconds of available burst data in each XY, XZ grid square. EHs clearly occur mostly in the plasma wake and even show the same aberration with respect to the lunar optical shadow as the density. A small number of EHs (161) are scattered outside

the plasma wake ($|Y| > 3$ or $|Y| < 3$ and $X > 1$). Analysis of 16 of these events, chosen randomly from the 161, shows that they all occur within ~1,000 km of solar wind current sheets, consistent with prior studies of EH in the solar wind (Malaspina et al., 2013).

The data of Figure 4e close to the wake are now examined in more detail, referencing the location of each 1-s burst interval and identified EH to the center of the plasma wake. To account for variation of the depth and width of the plasma wake depending on solar wind conditions and the downstream distance of the wake crossing, the wake center and approximate width (σ) is found by fitting a Gaussian to the depression in proton density caused by the wake. Wake crossings without data bursts or whose wakes were shallower than 0.8 normalized density were removed from consideration (to eliminate ill-defined wake crossings), as were any burst or EH events less than 3 R_M downwake and EH events more than 2 R_M radial distance from the optical wake center line. There remains a data set of 385 wake crossings.

Figure 5a shows a histogram of the number of EHs as a function of normalized time t/σ (and hence approximately normalized Y distance) from the wake center. There is a pronounced depression in EH counts near the wake center, and a fast fall-off outside the wake. The data burst profile, by contrast, is peaked near the center and somewhat broader (Figure 5b). Figure 5c shows a histogram of the number of EH events per second as a function of distance from the wake center. The hollowness of EH occurrence near the wake center is emphasized further by this normalization. Detailed specification of the holes analyzed and data relating to the theory is provided in the supporting information.

5. Discussion and Conclusions

The observations confirm the theoretical prediction that the lunar wake should be a region of concentrated electrostatic instability and EH production. The possibility of hole generation by other mechanisms is not ruled out since there are many, and complexities such as wake nonstationarity might also be important, but the dimple forming process will be operative. A theoretical prediction of the absolute level of hole flux to be observed would require some assumption about how long holes persist. They are expected to break up by the transverse instability (Muschietti et al., 2000; Singh, 2003) because the electron cyclotron frequency is much less than the plasma frequency. The fact that the observed hole flux falls fairly quickly toward the wake edge, is evidence that holes do break up, because otherwise the flux would be approximately uniform outside the hole production region. Moreover, the holes our rigorous observational filter selects (giving rate $\lesssim 0.5/s$) certainly strongly under-represent the total hole flux. Therefore we cannot yet meaningfully compare theory with the absolute hole observation rate. Nevertheless, the hollow hole flux profile observed is qualitatively consistent with prediction.

Acknowledgments
The authors thank the entire THEMIS/ARTEMIS team, and specifically the EFI and ESA teams for their support, and C. Zhou for helpful discussions. This work was funded by NASA award NNX16AG82G. All data used in this work are available on the THEMIS/ARTEMIS archive: http://themis.ssl.berkeley.edu/data/themis/.

References

Andersson, L., Ergun, R. E., Tao, J., Roux, A., Lecontel, O., Angelopoulos, V., et al. (2009). New features of electron phase space holes observed by the THEMIS mission. *Physical Review Letters*, *102*(22), 225004. https://doi.org/10.1103/PhysRevLett.102.225004

Angelopoulos, V. (2011). The ARTEMIS Mission. *Space Science Reviews*, *165*, 3–25. https://doi.org/10.1007/s11214-010-9687-2

Bernstein, I. B., Greene, J. M., & Kruskal, M. D. (1957). Exact nonlinear plasma oscillations. *Physical Review*, *108*(4), 546–550.

Birch, P. C., & Chapman, S. C. (2001). Particle-in-cell simulations of the lunar wake with high phase space resolution. *Geophysical Research Letters*, *28*(2), 219–222.

Bonnell, J. W., Mozer, F. S., Delory, G. T., Hull, A. J., Ergun, R. E., Cully, C. M., et al. (2008). The Electric Field Instrument (EFI) for THEMIS. *Space Science Reviews*, *141*(1–4), 303–341. https://doi.org/10.1007/s11214-008-9469-2

Cully, C. M., Ergun, R. E., Stevens, K., Nammari, A., & Westfall, J. (2008). The THEMIS Digital Fields Board. *Space Science Reviews*, *141*, 343–355. https://doi.org/10.1007/s11214-008-9417-1

Ergun, R. E., Carlson, C. W., McFadden, J. P., Mozer, F. S., Muschietti, L., Roth, I., & Strangeway, R. J. (1998). Debye-scale plasma structures associated with magnetic-field-aligned electric fields. *Physical Review Letters*, *81*, 826–829. https://doi.org/10.1103/PhysRevLett.81.826

Ergun, R. E., Tucker, S., Westfall, J., Goodrich, K. A., Malaspina, D. M., Summers, D., et al. (2016). The axial double probe and fields signal processing for the MMS mission. *Space Science Reviews*, *199*, 167–188. https://doi.org/10.1007/s11214-014-0115-x

Fairfield, D. H. (1971). Average and unusual locations of the Earth's magnetopause and bow shock. *Journal of Geophysical Research*, *76*, 6700–6716. https://doi.org/10.1029/JA076i028p06700

Haakonsen, C. B., Hutchinson, I. H., & Zhou, C. (2015). Kinetic electron and ion instability of the lunar wake simulated at physical mass ratio. *Physics of Plasmas*, *22*(3), 32311. https://doi.org/10.1063/1.4915525

Hutchinson, I. H. (2012). Electron velocity distribution instability in magnetized plasma wakes and artificial electron mass. *Journal of Geophysical Research*, *117*, A03101. https://doi.org/10.1029/2011JA017119

Hutchinson, I. H. (2017). Electron holes in phase space: What they are and why they matter. *Physics of Plasmas*, *24*(5), 55601. https://doi.org/10.1063/1.4976854

Hutchinson, I. H., Haakonsen, C. B., & Zhou, C. (2015). Non-linear plasma wake growth of electron holes. *Physics of Plasmas*, *22*(3), 32312. https://doi.org/10.1063/1.4915526

Malaspina, D. M., Newman, D. L., Willson, L. B., Goetz, K., Kellogg, P. J., & Kerstin, K. (2013). Electrostatic solitary waves in the solar wind: Evidence for instability at solar wind current sheets. *Journal of Geophysical Research: Space Physics*, *118*, 591–599. https://doi.org/10.1002/jgra.50102

Matsumoto, H., Deng, X. H., Kojima, H., & Anderson, R. R. (2003). Observation of Electrostatic Solitary Waves associated with reconnection on the dayside magnetopause boundary. *Geophysical Research Letters*, *30*(6), 1326. https://doi.org/10.1029/2002GL016319

Matsumoto, H., Kojima, H., Miyatake, T., Omura, Y., Okada, M., Nagano, I., & Tsutsui, M. (1994). Electrostatic solitary waves (ESW) in the magnetotail: BEN wave forms observed by GEOTAIL. *Geophysical Research Letters*, *21*(25), 2915–2918. https://doi.org/10.1029/94GL01284

McFadden, J. P., Carlson, C. W., Larson, D., Ludlam, M., Abiad, R., Elliott, B., et al. (2008). The THEMIS ESA plasma instrument and in-flight calibration. *Space Science Reviews*, *141*(1–4), 277–302. https://doi.org/10.1007/s11214-008-9440-2

Muschietti, L., Roth, I., Carlson, C. W., & Ergun, R. E. (2000). Transverse instability of magnetized electron holes. *Physical Review Letters*, *85*(1), 94–97.

Penrose, O. (1960). Electrostatic instabilities of a uniform non-Maxwellian plasma. *Physics of Fluids*, *3*(2), 258–265. https://doi.org/10.1063/1.1706024

Rubia, R., Singh, S. V., & Lakhina, G. S. (2017). Occurrence of electrostatic solitary waves in the lunar wake. *Journal of Geophysical Research: Space Physics*, *122*, 9134–9147. https://doi.org/10.1002/2017JA023972

Singh, N. (2003). Space-time evolution of electron-beam driven electron holes and their effects on the plasma. *Nonlinear Processes in Geophysics*, *10*, 53–63.

Zhang, H., Khurana, K. K., Kivelson, M. G., Angelopoulos, V., Wan, W. X., Liu, L. B., et al. (2014). Three-dimensional lunar wake reconstructed from ARTEMIS data. *Journal of Geophysical Research: Space Physics*, *119*, 5220–5243. https://doi.org/10.1002/2014JA020111